Thin Solid Films 573 (2014) 67–73

Contents lists available at ScienceDirect

Thin Solid Films

journal homepage: www.elsevier.com/locate/tsf

Icephobicity of polydimethylsiloxane-*b*-poly(fluorinated acrylate)

Hui Li [a,b,c,1], Xiaohui Li [a,b,1], Chenghao Luo [a,b], Yunhui Zhao [a,b], Xiaoyan Yuan [a,b,*]

[a] School of Materials Science and Engineering, Tianjin University, Tianjin 300072, China
[b] Tianjin Key Laboratory of Composite and Functional Materials, Tianjin 300072, China
[c] School of Chemistry and Chemical Engineering, Shandong Key Laboratory of Fluorine Chemistry and Chemical Engineering Materials, University of Jinan, Jinan 250022, China

ARTICLE INFO

Article history:
Received 7 May 2014
Received in revised form 28 October 2014
Accepted 3 November 2014
Available online 8 November 2014

Keywords:
Polydimethylsiloxane
Poly(fluorinated acrylate)
Block copolymer
Icephobicity
Synergistic effect of silicon and fluorine

ABSTRACT

A facile process to fabricate icephobic surfaces was developed by spin-coating the polydimethylsiloxane-*b*-poly(fluorinated acrylate) (PDMS-*b*-PFA) block copolymers on the substrate. The surface microstructure and chemical composition of the block copolymer films can be adjusted by changing the PDMS content. Icephobic properties of the copolymer surface were mainly ascribed to "flexible-hard" microphase separation and the ratio of fluorine to silicon. The appropriate microphase domain size and the fluorine/silicon ratio could weaken the interaction of ice and copolymer surface and delay icing of water droplets on the copolymer surface. The copolymers containing 15 wt.% PDMS showed the most outstanding icephobicity by depressing the interaction between ice and the copolymer surface.

1. Introduction

Excessive ice accretion on the surfaces of power and communication networks, aircraft and ships might lead to undesired service outages or costly safety issues [1]. An ideal solution would be preventing ice accumulation rather than de-icing which is time-consuming and expensive. This could be accomplished by depositing icephobic coatings [2,3].

Low surface energy coatings including fluorinated and organic silicone materials have been studied for decades to prepare anti-icing coatings [4–7]. Generally, the interactions between the substance and ice include electrostatic force, hydrogen bonding and mechanical adhesion. Due to the flexible mobility of polydimethylsiloxane (PDMS) chains at lower temperatures, the PDMS-based polymer can prevent mechanical adhesion and reduce ice adhesion strength, which makes it a good candidate for icephobic coatings. Because of the low dielectric constant ($\varepsilon \approx 2.1$), fluoropolymer can also reduce the electrostatic force between the substrate and ice, resulting in low ice adhesion strength [3]. However, the interaction energy between the fluorocarbon group and water is three times larger than that between the siloxane group and water [8]. The water droplet could hardly slide on the surface of the fluoropolymer because of the strong interaction between fluorocarbon groups and water. For a heterogeneous polymer surface containing both fluorocarbon and siloxane, the interaction energies between the polymer surface and water would be decreased when both fluorocarbon group and siloxane group close into a water molecule. Thus, the synergistic effect of silicon and fluorine would contribute to the reduction of contact angle hysteresis and lead to low ice adhesion strength [8].

At the present, relative reports have shown that certain microstructures of the coating surface could contribute to improving anti-icing performances [9,10]. The surface morphology can have a spectacular influence on hydrophobicity and icephobic behaviors. For example, in Cassie–Baxter state, a water drop can be supported by air which is jammed between the water drop and the rough surface of the substrate [11]. In such aspect, water drops tend to behave like pearls and can roll down from the surface. It was well known that the incompatibility of block compositions could result in microphase separation both in bulk and on surface of the block copolymers. Usually, the domain size of microphase on the block copolymer surface generated by self-assembly could be controlled from 5 nm to 100 nm, but it also could be as large as several microns by selecting proper materials and methods [12].

In this paper, the polydimethylsiloxane-*b*-poly(fluorinated acrylate) block copolymers (PDMS-*b*-PFA) with various PDMS contents were synthesized by radical solution polymerization using PDMS macroazoinitiator (PDMS-MAI), and microphase separation, surface elements composition and roughness, wettabilities and icephobic properties of PDMS-*b*-PFA were systematically studied. It was assumed that the anti-icing properties of the block copolymer strongly relied on both the domain size of microphase and the ratio of fluorine to silicon on the surface. The appropriate microphase domain size and fluorine/

* Corresponding author. Tel./fax: +86 22 8740 1870 (O).
E-mail addresses: yuanxy@tju.edu.cn, xyuan28@yahoo.com (X. Yuan).
[1] Hui Li and Xiaohui Li contributed equally to this work.

http://dx.doi.org/10.1016/j.tsf.2014.11.007
0040-6090/

silicon ratio could weaken the interaction of ice and copolymer surface and delay icing of a water droplet on the copolymer surface.

2. Experimental methods

2.1. Materials

α,ω-Dihydrogen-terminated polydimethylsiloxane (H-PDMS-H) with molecular weight of about 12,500 was supplied by Hangzhou Silong Material Technology Co., Ltd., China. 4,4′-Azobis(4-cyanovaleric acid) was purchased from Aldrich. 2,2,3,3,4,4,5,5,6,6,7,7-Dodecafluoroheptyl methacrylate (DFHMA) was supplied by Xeogia Fluorin-Silicon Chemical Co., Ltd., China. Methy1methacrylate (MMA), *n*-butyl acrylate (*n*BA), hydroxyethyl methacrylate (HEMA) and solvents were purchased from Tianjin Kemiou Chemical Reagent Co., Ltd., China. All the monomers were treated with 5 wt.% aqueous NaOH to remove inhibitor, dried overnight with anhydrous sodium sulfate and stored at low temperature prior to use.

2.2. Synthesis

PDMS macroazoinitiator (PDMS-MAI) was synthesized as shown in our previous report [13]. Briefly, PDMS-MAI was prepared by esterification with hydroxyl terminated PDMS (HO-PDMS-OH) with 4,4′-azobis(4-cyanovaleric acid), whereas HO-PDMS-OH was synthesized by hydrosilylation of allyl alcohol and H-PDMS-H by using a platinum catalyst. The PDMS-*b*-PFA block copolymers with various PDMS contents were prepared by radical solution polymerization using PDMS-MAI. The polymerization was carried out under nitrogen atmosphere in a 250-mL four-neck flask equipped with reflux condenser, mechanical stirrer, dropping funnel and a nitrogen inlet. The monomer compositions were listed in Table 1. After MMA, *n*BA and HEMA were polymerized using PDMS-MAI as the initiator in MIBK at 60 °C for 4 h, DFHMA was added drop-by-drop within 1 h. Afterward, the reaction mixture was stirred for another 5 h at 65 °C. The reaction was stopped by cooling to room temperature. The prepared copolymers were purified by dissolution and reprecipitation with tetrahydrofuran (THF) and hexane, respectively. The PDMS-*b*-PFA copolymer was soluble in THF but insoluble in hexane, whereas the poly(fluorinated acrylate) (PFA) homopolymer was insoluble in THF. After several cycles of the dissolution and reprecipitation process, the PDMS-*b*-PFA copolymer was purified, and then dried under vacuum at 40 °C for 24 h.

2.3. Preparation of the PDMS-b-PFA film

The PDMS-*b*-PFA films were prepared by spin-coating of the copolymer solution in ethyl acetate on the substrate at room temperature. The spinning speed was set at 300 rpm (6 s) and 2000 rpm (10 s) for the first and second steps, respectively. The thickness of the copolymer films was around 210 ± 15 nm.

2.4. Characterizations

Fourier transform infrared (FT-IR) spectra of samples were recorded between 4000 cm^{-1} and 400 cm^{-1} in an AVATER-360B spectrophotometer using KBr pellet technique.

^1H nuclear magnetic resonance (^1H NMR) measurements were carried out in Varian machines (INOVA 500 MHz and Infinity plus 300WB, USA) by dissolving the samples in deuteriochloroform or deuterated dimethyl sulfoxide.

The molecular weight and polydispersity of the prepared PDMS-*b*-PFA copolymers were determined in a Waters 1515–2414 gel permeation chromatography (GPC) with THF as the eluent flowing at 1 mL/min. Polystyrene standards were used to generate a calibration curve.

Differential scanning calorimetry (DSC) measurements were carried out with a DSC200F3 differential scanning calorimeter (NETZSCH, Germany) under N_2 atmosphere at a heating rate of 10 °C min^{-1} from −150 °C to 150 °C.

Atomic force microscope (AFM) experiments were performed using an AFM machine (CSPM5500A of Ben Yuan Ltd., China) equipped with E-type vertical engage piezoelectric scanner and operated in a tapping-mode at room temperature.

Copolymer morphologies were also observed under a transmission electron microscope (TEM) (JEOL JEM100CXII 100 kV, Japan). The diluted copolymer solution was deposited onto a copper net and stained with ruthenium tetroxide (RuO_4) vapor for 2 h.

The surface chemical composition of the PDMS-*b*-PFA copolymer film was measured by X-ray photoelectron spectroscopy (XPS, Perkin-Elmer PHI 5000C ECSA) using at a 90° take-off angle under an ultra-high vacuum less than 6.7×10^{-6} Pa at 45° with Al K radiation (1486.6 eV) operating at 24.2 W. The tested area was a circle of 100 μm diameter.

Water contact angles and contact angle hysteresis on the surfaces were measured in a modified optical contact angle meter system with a cold plate (JC2000D, Shanghai Zhongchen Equipment Ltd., China). A droplet of distilled water (5 μL) was placed on the sample surface and then expanded or shrunk at a flow rate in the range of 0.1–1.0 μL/s via a syringe needle. Images of the droplets were captured by a CCD camera and analyzed to obtain the advancing and receding contact angles, and values of the water contact angle hysteresis were calculated [13]. The surface energies of the polymers were evaluated by measuring the static water and hexadecane contact angles on the surface [13]. All the presented values are averages of at least five or six measurements each. The modified optical contact angle meter system with a high speed CCD camera was also utilized to observe the freezing profiles of individual water droplets on sample substrates at −20 °C. The freezing process of water droplets in 4 μL was recorded by the high speed CCD camera at a speed of 25 fps. The sample substrates were mounted on a cold plate controlled at −20 °C under nitrogen (relative humidity <10%). The icing delay time of the water droplet on the copolymer surfaces was recorded as the start time of freezing.

Ice adhesion strength was measured using a universal testing machine (QJ211, Shanghai Qingji Instrumentation Science and Technology Co., Ltd., China) equipped with a 100 N load cell (Transcell Technology,

Table 1
Compositions, molecular weight and polydispersity index, and yields of the prepared PDMS-*b*-PFA copolymers.

Sample	PDMS-MAI (wt.%)	Monomer (g)				$\overline{M}_n$ ($\times 10^4$)	$\overline{M}_w$ ($\times 10^4$)	$\overline{M}_w/\overline{M}_n$	Yield (%)
		MMA	*n*BA	HEMA	DFHMA				
HO-PDMS-OH	–	–	–	–	–	1.25	2.14	1.71	–
PDMS-MAI	–	–	–	–	–	2.17	3.31	1.53	–
PF1	50	6	4.5	1.5	3	2.73	4.12	1.51	78.3
PF2	40	6	4.5	1.5	3	2.85	7.04	2.47	68.6
PF3	30	6	4.5	1.5	3	4.11	6.83	1.66	54.2
PF4	15	6	4.5	1.5	3	6.42	11.29	1.75	43.9

Inc., USA) in a pull off mode. As shown in our previous report, the aluminum spindle in 20 mm diameter was etched in diluted hydrochloric acid to attain a rough surface which would not be separated from ice during testing [13].

The ice shear strength was measured on a costumed-made cooling stage which could hold a 4 × 4 array of samples [14]. The coated Al plates (20 mm × 20 mm) were placed onto the cooling stage and let the copolymer film upwards. The glass columns were put on the Al plates and filled with 450 μL of fresh deionized water. Each column had a contact area with the Al plate of approximately 78.5 mm^2. The cooling stage was covered by an organic glass box which was purged with nitrogen gas to decrease the humidity. The temperature of the stage reached to −15 °C at a rate of 2 °C/min and was kept for 3 h. A force transducer (Imada ZP-500N, Japan) was mounted on a motion stage which moved forward at a rate of 0.5 mm/s to the glass columns. The maximum force was recorded for determining the ice adhesion strength by dividing the area between ice and the contact polymer surface. The average values and the standard deviation were obtained from nine parallel samples.

3. Results and discussion

PDMS-MAI was firstly prepared by esterification with hydroxyl terminated PDMS with 4,4′-azobis(4-cyanovaleric acid). Then, PDMS-*b*-PFA copolymers were synthesized using PDMS-MAI in 15–50% of mass percentage (Table 1) and the synthesis route was shown in Scheme 1. FT-IR spectra of the PDMS-*b*-PFA copolymers are shown in Fig. 1. As shown in Fig. 1, the strong absorption peak at 1730 cm^{-1} was assigned to C═O stretching vibration. Absorption peaks at 1260 cm^{-1} and 800 cm^{-1} belong to the stretching vibration of Si–CH_3 and the bending vibration of Si–O, respectively. The asymmetric stretching vibration peaks of Si–O–Si appear at 1020 cm^{-1}. The characteristic absorption peaks at 690 cm^{-1} for wagging vibrations of CF_2 groups was observed. The stretching vibration peak of C═C at 1640 cm^{-1} disappeared, suggesting that there were no more redundant monomers in reaction products.

Characterization by ^{1}H NMR was performed for PF3 as a typicality of the PDMS-*b*-PFA copolymers. In Fig. 2, weak characteristic signals of δ_H in O–CH_2– and –CFH– in DFHMA were found at 4.5 ppm and 5.5 ppm, respectively. The peaks at 3.6–4.0 ppm were the contribution of methylene protons close to oxygen atom of ester bond. The signal of δ_H in PDMS was observed at 0.1 ppm for the -Si–CH_3 group. No peaks for the protons associated to double bond of MMA, *n*BA, HEMA and DFHMA were detected in the ^{1}H NMR spectrum of the PF3 copolymer.

The number-average molecular weight of the PDMS-*b*-PFA copolymers was about 2.73–6.42 × 10^4, and the polydispersity index of them was in range of 1.70–2.47 (Table 1). Only one peak was detected at a retention volume of GPC (Fig. 3), demonstrating that the PDMS-*b*-PFA copolymers were obtained. The yield of the block copolymers increased with the increase of the PDMS-MAI content (Table 1).

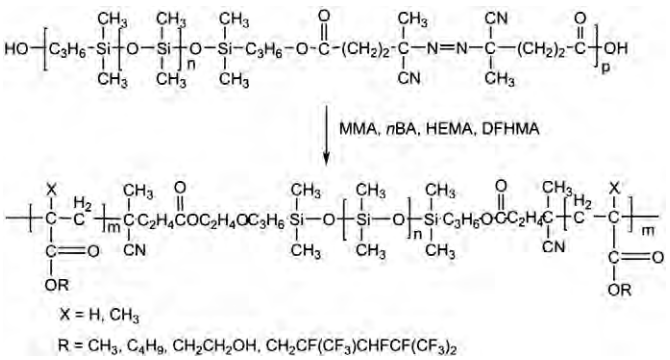

Scheme 1. Synthesis of the PDMS-*b*-PFA block copolymers.

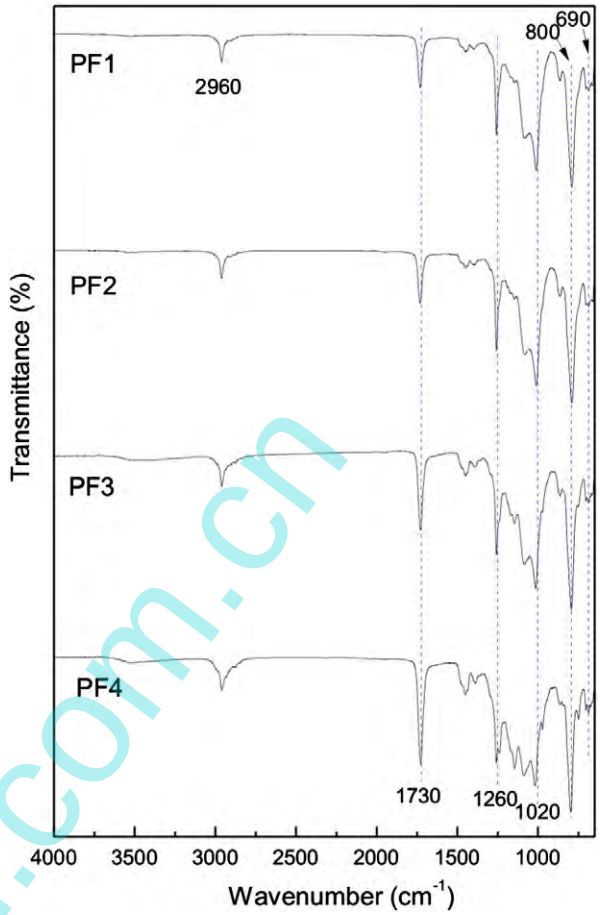

Fig. 1. FT-IR spectra of the PDMS-*b*-PFA copolymers.

The thermal transitions of the PDMS-*b*-FAC copolymers were investigated by DSC as shown in Fig. 4. Two glass transitions were observed for all the copolymers. Glass transition temperature at about −125 °C (T_{g1}) attributed to the PDMS block was detected in all the copolymer thermograms, whereas the melting peak at about −40 °C also assigned by the PDMS block was only found in the curves of PF1, PF2 and PF3. The PFA block displayed its T_{g2} at about 45 °C higher than that of PDMS. The DSC results suggested that there were possibly incompatible components in all the prepared PDMS-*b*-PFA copolymers that could lead to microphase separation.

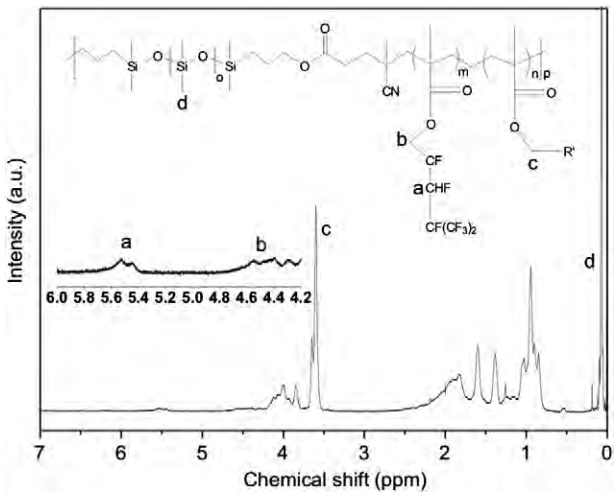

Fig. 2. ^{1}H NMR spectrum of PF3, showing a typicality of the PDMS-*b*-PFA copolymers.

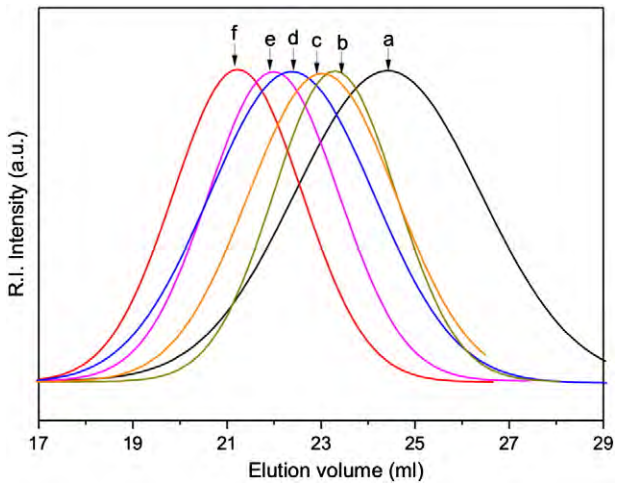

Fig. 3. GPC curves of PDMS-OH (a), PDMS-MAI (b), PF1 (c), PF2 (d), PF3 (e) and PF4 (f).

A given amount of block copolymers were dissolved in ethyl acetate to prepare a 20 wt.% solution, and the block copolymer films were prepared by spin-coating on the substrate at room temperature. The surface topology and roughness of the block copolymers with various PDMS contents were examined by AFM. As seen from Fig. 5, all of the block copolymers demonstrated distinct microphase separation, but the morphologies were different from each other, and strongly dependent upon the PDMS content [15]. The domain sizes caused by the microphase separation on surfaces of PF1, PF2, PF3 and PF4 were 90–200 nm, 50–150 nm, 20–90 nm and 40–65 nm, respectively, decreasing with the reduced PDMS content in the block copolymers. The surface roughness (S_q) of the copolymer films also differed from each other, but the discrepancy was not obvious. As shown in Table 2, the block copolymer PF1 with the highest PDMS content showed the largest surface roughness of 1.61 nm. Because of the thermodynamic incompatibility of the PDMS-*b*-PFA block copolymers, the PDMS block tended to be assembled into a larger area and formed a rough surface.

The surface as well as the interior of PDMS-*b*-PFA block copolymers could present microphase-separated structures due to the partial incompatibility between PDMS and PFA blocks. It has been reported that the PDMS rich phase was easily stained by RuO_4, while the polyacrylate rich phase was not [16]. To investigate the microphase structures of the PDMS-*b*-PFA block copolymers with different contents of PDMS, thin films of those copolymers stained by RuO_4 were observed under TEM as shown in Fig. 6. It can be seen that all of the block copolymers showed

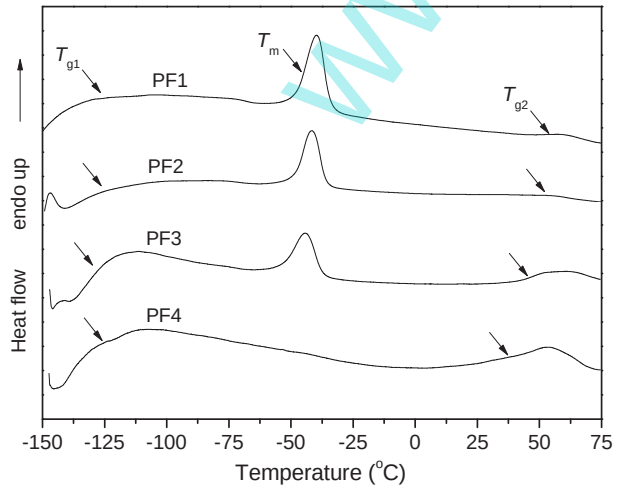

Fig. 4. DSC curves of the PDMS-*b*-PFA copolymers: PF1, PF2, PF3 and PF4.

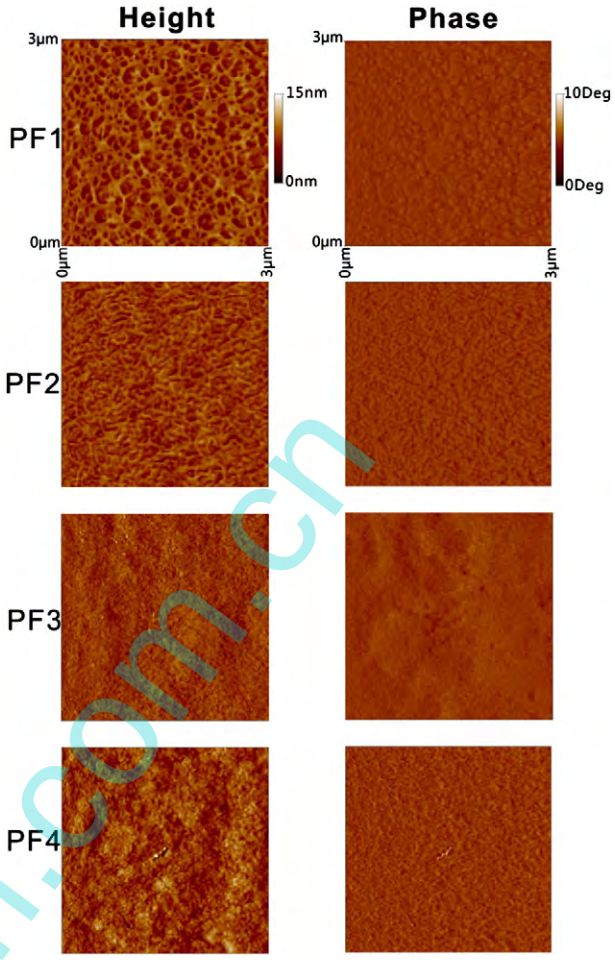

Fig. 5. AFM topography and phase images of the PDMS-*b*-PFA copolymer films over a scope of 3 μm × 3 μm.

distinct microphase-separated structures. The microphase morphology changed from island shapes (PF1 and PF2) to bicontinuous shapes (PF3 and PF4), and the domain size decreased with the decrease of the PDMS content from PF1 to PF4 in accordance with the results observed by AFM (Fig. 5).

The surface elemental compositions of the PDMS-*b*-PFA copolymer films were evaluated by XPS and the percentages of carbon, oxygen, silicon and fluorine were collected in Table 2. The percentage of silicon element on the PF1 (the block copolymer with 50 wt.% PDMS) surface was about 21.0% (Table 2), while the fluorine element was not observed on the corresponding copolymer surface, suggesting the migration of PDMS chains onto the surface. With the decrease of the PDMS content, the percentage of fluorine element gradually increased. The fluorine percentage on the PF4 (with 15 wt.% PDMS) surface reached 6.7% and the silicon percentage decreased to 10.4% (Table 2). Based on the AFM data (Table 2), the surface roughness decreased from PF1 to PF3 (1.61 nm to 0.80 nm) as the amount of PDMS content decreased, whereas PF4 showed increased surface roughness (1.38 nm). It is assumed

Table 2
Surface roughness (S_q) analyzed by AFM and the element compositions of the PDMS-*b*-PFA copolymer surfaces obtained by XPS.

Sample	S_q (nm)	C (atomic %)	O (atomic %)	F (atomic %)	Si (atomic %)	F/Si ratio
PF1	1.61	53.4	25.7	–	21.0	–
PF2	1.01	54.2	25.0	1.5	19.3	0.08
PF3	0.80	58.2	24.3	2.8	14.7	0.19
PF4	1.38	59.7	23.2	6.7	10.4	0.64

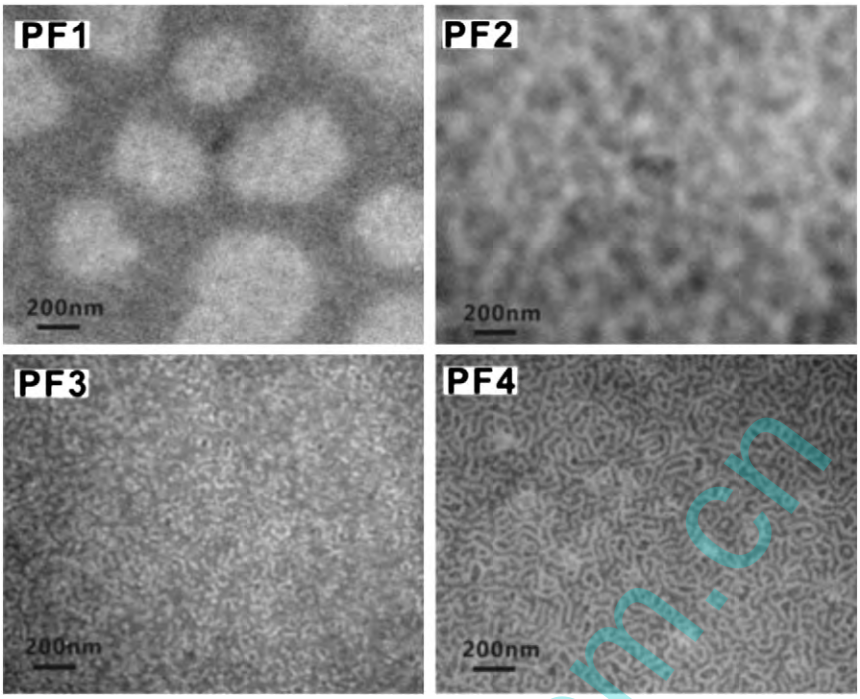

Fig. 6. TEM micrographs of the PDMS-*b*-PFA copolymers.

that the surface roughness could be enhanced by the enrichment of fluorinated polyacrylate block on the copolymer surface. Therefore, it could be concluded that although both of the fluorinated polyacrylate and PDMS blocks had the ability of migrating toward the surface, the PDMS block was easier to move onto the surface than the fluorinated polyacrylate block due to the better flexibility of the organic silicone chain [17].

In order to analyze the wetting properties of the block copolymers, the water contact angle, water contact angle hysteresis and surface energy were measured and shown in Fig. 7a. The surface energy of all the samples was less than 27 mJ/m^2 and significantly lower than that of polyacrylate (39 mJ/m^2 for poly(methyl methacrylate)) [17], suggesting good hydrophobic properties. Among them, sample PF4 exhibited the highest water contact angle (109°) as well as the lowest surface energy (23.9 mJ/m^2). It could be mainly ascribed to the enrichment of fluorine on copolymer surface and the bigger surface roughness (1.38 nm) compared with PF2 (1.01 nm) and PF3 (0.80 nm). To some extent, the water contact angle hysteresis could reflect the interaction force between the polymer surface and water. Usually, the smaller the contact angle hysteresis exhibits, the weaker the interaction force is. It could be seen from Fig. 7a that the water contact angle hysteresis varied in range of 22–46° for all the samples, and decreased with the increase of fluorine element content of the copolymer surface from PF1 (46.1 ± 4.98°) to PF4 (21.2 ± 3.05°). It could also be assumed that in the condition of the similar roughness and microstructures of the copolymer surface, chemical composition especially synergistic effect of silicon and fluorine could be the main reason of the decrease of water contact angle hysteresis [3,9,18].

Essentially, the interaction between the polymer surface and water is mainly dominated by the competition between the cohesion forces among the water molecules in the water droplet and the adhesion forces with the solid surface. Therefore, the interaction force was also investigated by monitoring the evolution of water droplet evaporation on the copolymer surfaces [19]. Changes in the contact angle for water droplets as they evaporated on the copolymer surfaces were measured

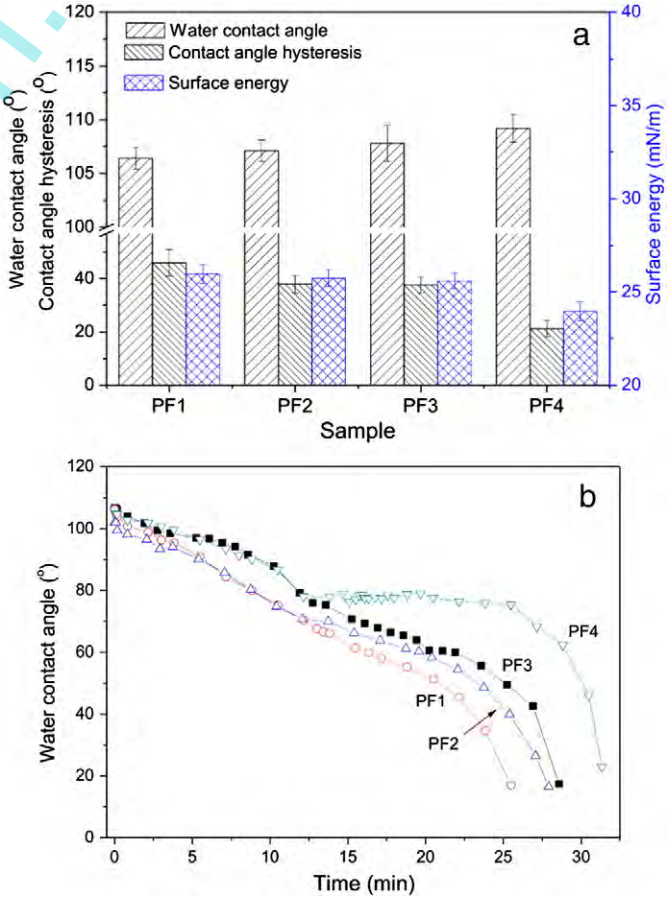

Fig. 7. (a) Water contact angles, contact angle hysteresis and surface energies and (b) evolution of the contact angle of a 4-μL water droplet at 25 °C on the surfaces of the PDMS-*b*-PFA copolymers.

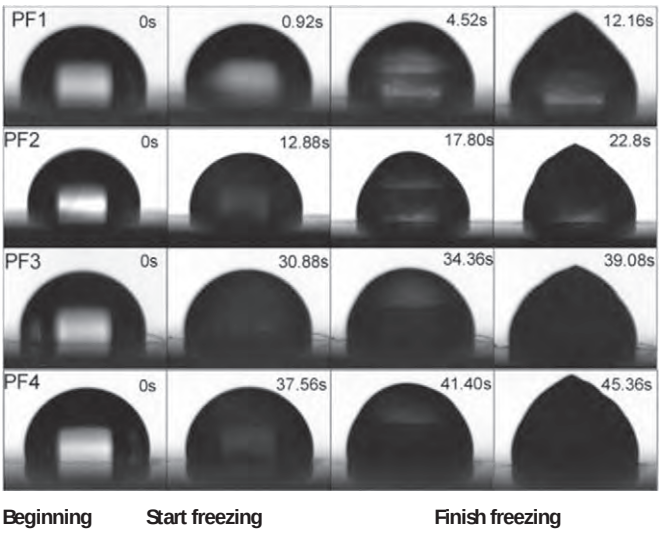

Fig. 8. Observation of the freezing process of water droplets on the surface of the PDMS-*b*-PFA copolymers at −20 °C.

as shown in Fig. 7b. At the beginning, contact angles of the water droplet on all the sample surfaces decreased steadily till ~12 min. In this evaporation stage, the height of the water droplet dwindled gradually while the diameter of its contact region remained almost a constant, suggesting that water diffusion (evaporation) overwhelmed the cohesion force among the water molecules [19]. After then, a slow decrease in contact angles was observed till ~22 min, which resulted from the contact diameter reduction of water droplet, further indicating that water evaporation surmounted not only the cohesion force but also the adhesion force on the surface. Among all the four samples, the changes of the contact angle of the droplet on the copolymer surfaces were captured by a high speed. The variation of the contact angle on the sample PF4 surface was the slowest, indicating that the interaction between the PF4 surface and water was the smallest. This trend was also in accordance with that of the contact angle hysteresis.

Water droplets in 4 μL were deposited on the block copolymer surfaces at −20 °C and the freezing profiles of the individual water CCD camera as shown in Fig. 8. The icing delay times of the water droplet on the PF1, PF2, PF3 and PF4 surfaces were 0.92 s, 12.88 s, 30.88 s and 37.56 s, respectively, showing an increasing tendency with the decreased PDMS content. As could be concluded from the results of icing delay time and AFM images, the microphase-separated structures might affect the ice nucleation rate due to the increase of free energy barrier for the formation of a critical nucleus at the interface [9,20]. Moreover, it should also be noted that the lower the contact angle hysteresis, the longer the icing delay time, demonstrating that the contact angle hysteresis might be one of the parameters affecting the delay time during ice formation [21].

From a practical application point of view, the ice adhesion and shear strengths on the block copolymer surfaces were also examined (Fig. 9). It could be seen that the ice adhesion strength on the block copolymer surfaces varied from ~28 kPa to ~17 kPa. With the same trend of the ice adhesion strength, the ice shear strength tended to decrease from ~305 kPa to ~187 kPa with the reduction of the PDMS content from 50 wt.% to 15 wt.%, significantly lower than the value of the ice adhesion and shear strengths on a commercial polyacrylate–polyurethane coating (~35 kPa and ~1200 kPa, respectively). Among all the copolymers, both of the ice adhesion and shear strength values for PF4 were the smallest, exhibiting good icephobic properties, which was mainly attributed to the surface microphase-separated structures and chemical composition of the block copolymers (synergistic effect of silicon and fluorine) [22–24]. The microphase separation of PF4 was related to the enrichment of PDMS and fluorinated polyacrylate blocks on the

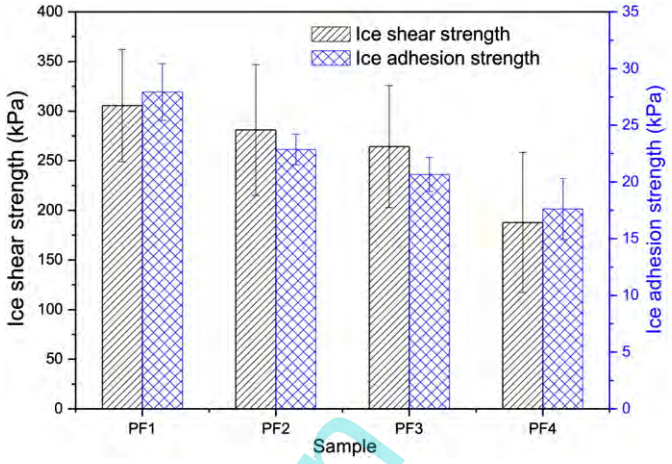

Fig. 9. Ice adhesion and ice shear strengths of the PDMS-*b*-PFA copolymers.

copolymer surface. Based on the AFM result (Table 2), the surface roughness of PF4 (1.38 nm) was bigger than those of other samples except for PF1 which contains little fluorine on its surface. The bigger surface roughness could lead to a small contact area between the water and copolymer surface, resulting in lower ice adhesion and shear strengths. From the XPS result (Table. 2), with the decrease of the PDMS content, the percentage of fluorine element gradually increased, and the F/Si values (0.64) of the sample PF4 was higher than other samples. The high F/Si value of the sample PF4 can result in an enhanced synergistic effect of fluorine and silicon, thereby leading to low ice adhesion and shear strengths [3,8]. Moreover, PDMS-*b*-PFA was composed of PDMS block and the fluorinated polyacrylate block, and both blocks were all easy to migrate to the surface due to their low surface energy, leading to "flexible-hard" microphase-separated structures on the surface under appropriate conditions. The ice/copolymer interface could easily result in "stress concentration" under stress condition, which would further reduce the ice adhesion and shear strengths.

4. Conclusions

The PDMS-*b*-PFA block copolymers with different PDMS contents were synthesized by radical solution polymerization using PDMS macroazoinitiator. Microphase separation, surface element composition and roughness, wettabilities and icephobic properties of PDMS-*b*-PFA were systematically studied. It was found that with the decrease of the PDMS content from 50 wt.% (PF1) to 15 wt.% (PF4), the domain sizes caused by surface microphase separation decreased from 90–200 nm to 40–65 nm, and the contact angle hysteresis also reduced from 46.1 ± 4.98° to 21.2 ± 3.05°. Besides, from PF1 to PF4, the ice adhesion and shear strengths showed a decreasing tendency from ~28 kPa and ~305 kPa down to ~17 kPa and ~187 kPa, respectively. PF4 with 6.7% fluorine and 10.4% silicon on the surface exhibited the most outstanding icephobic properties mainly ascribed to the "flexible-hard" microphase-separated structures on the surface and the synergistic effect of silicon and fluorine.

Acknowledgments

This work is financially supported by the National Natural Science Foundation of China (Nos. 51273146 and 51103061) and Natural Science Foundation of Tianjin, China (No. 14ZCZDGX00008).

References

[1] J. Meuler, J.D. Smith, K.K. Varanasi, J.M. Mabry, G.H. McKinley, R.E. Cohen, Relationships between water wettability and ice adhesion, ACS Appl. Mater. Interfaces 2 (2010) 3100.

[2] A.J. Meuler, G.H. Mckinley, R.E. Cohen, Exploiting topographical texture to impart icephobicity, ACS Nano 4 (2010) 7048.
[3] R. Menini, M. Farzaneh, Advanced icephobic coatings, J. Adhes. Sci. Technol. 25 (2011) 971.
[4] H. Wang, G. He, Q. Tian, Effects of nano-fluorocarbon coating on icing, Appl. Surf. Sci. 258 (2012) 7219.
[5] Y. Huang, M. Hu, S. Yi, Preparation and characterization of silica/fluorinated acrylate copolymers hybrid films and the investigation of their icephobicity, Thin Solid Films 520 (2012) 5644.
[6] L. Zhu, J. Xue, Y. Wang, Q. Chen, J. Ding, Q. Wang, Ice-phobic coatings based on silicon-oil-infused polydimethylsiloxane, ACS Appl. Mater. Interfaces 5 (2013) 4053.
[7] J. Li, Y. Zhao, J. Hu, Anti-icing performance of a superhydrophobic PDMS/modified nano-silica hybrid coating for Insulators, J. Adhes. Sci. Technol. 26 (2012) 665.
[8] H. Murase, K. Nanishi, H. Kogure, T. Fujibayashi, K. Tamura, N. Haruta, Interactions between heterogeneous surfaces of polymers and water, J. Appl. Polym. Sci. 54 (1994) 2051.
[9] L. Cao, A.K. Jones, V.K. Sikka, J. Wu, D. Gao, Anti-icing superhydrophobic coatings, Langmuir 25 (2009) 12444.
[10] H. Li, Y.H. Zhao, X.Y. Yuan, Facile preparation of superhydrophobic coating by spraying a fluorinated acrylate random copolymer micelle solution, Soft Matter 9 (2013) 1005.
[11] L. Zhu, P. Shi, J. Xue, Y. Wang, Q. Chen, J. Ding, Q. Wang, Superhydrophobic stability of nanotube array surfaces under impact and static forces, ACS Appl. Mater. Interfaces 6 (2014) 8073.
[12] R.M. Ho, Y.W. Chiang, S.C. Lin, C.K. Chen, Helical architectures from self-assembly of chiral polymers and block copolymers, Prog. Polym. Sci. 36 (2011) 376.
[13] D.M. Yu, Y.H. Zhao, H. Li, H.Z. Qi, B. Li, X.Y. Yuan, Preparation and evaluation of hydrophobic surfaces of polyacrylate–polydimethylsiloxane copolymers for anti-icing, Prog. Org. Coat. 76 (2013) 1435.
[14] X.H. Li, Y.H. Zhao, H. Li, X.Y. Yuan, Preparation and icephobic properties of polymethyltrifluoropropylsiloxane–polyacrylate block copolymers, Appl. Surf. Sci. 316 (2014) 222.
[15] L. Feng, H. Fang, S. Zhou, L. Wu, One-step method for synthesis of PDMS-based macroazoinitiators and block copolymers from the initiators, Macromol. Chem. Phys. 207 (2006) 1575.
[16] E. Pouget, J. Tonnar, P. Lucas, L. Desmazes, F. Ganachaud, B. Boutevin, Well-architectured poly(dimethylsiloxane)-containing copolymers obtained by radical chemistry, Chem. Rev. 110 (2010) 1233.
[17] S.V. Chuppina, Anti-Icing gradient organosilicate coatings, Glas. Phys. Chem. 33 (2007) 502.
[18] C.W. Extrand, Y. Kumagai, An experimental study of contact angle hysteresis, J. Colloid Interface Sci. 191 (1997) 378.
[19] K.R. Khedir, G.K. Kannarpady, H. Ishihara, J. Woo, S. Trigwell, C. Ryerson, A.S. Biris, Advanced studies of water evaporation kinetics over teflon-coated tungsten nanorod surfaces with variable hydrophobicity and morphology, J. Phys. Chem. C 115 (2011) 13804.
[20] G. Peng, Y. Zheng, M. Wen, C. Song, Y. Lin, L. Jiang, Icephobic/anti-icing properties of micro/nanostructured surfaces, Adv. Mater. 24 (2012) 2642.
[21] A.S. Mohammad, S. Christopher, H. Scott, Effects of contact angle hysteresis on ice adhesion and growth on superhydrophobic surfaces under dynamic flow conditions, Colloid Polym. Sci. 291 (2013) 427.
[22] L.O. Andersson, C.G. Golander, S. Persson, Ice adhesion to rubber materials, J. Adhes. Sci. Technol. 8 (1994) 117.
[23] N.R. Byrd, Polysiloxane (amide-uride) anti-ice coating, US Pat. (2004) 6797795.
[24] R.B. Norman, P. Villa, G.K. Steven, Polysiloxane coatings for surfaces, US Pat. (2003) 0232201.